

Original Study

Open Access

Andrzej Helowicz*

Analysis of numerical models of an integral bridge resting on an elastic half-space

<https://doi.org/10.2478/sgem-2024-0026>

received April 17, 2024; accepted November 11, 2024.

Abstract: The paper presents three methods of the numerical modeling of a 60 m long integral bridge structure resting on an elastic half-space. For the analysis, three bridge models were built using Abaqus FEA software. Models A and C represent complex three-dimensional numerical models consisting of the bridge structure and the soil layer beneath it. The soil layer on which the bridge is resting was modeled as a homogeneous, isotropic, continuous, and elastic semi-infinite body elastic half-space. Model B represents a simple three-dimensional numerical model consisting of just the bridge structure. The stiffness of the soil layer beneath the structure in model B was modeled with spring constants derived for shallow footing foundation based on the theory for an elastic half-space. This model represents an engineering approach to the design of an integral bridge. In all models, the bridge deck is monolithically connected with abutment walls and intermediate piers. The bridge is made of cast-in-situ reinforced concrete. All material constants used in the analysis are presented in the table. Self-weight, uniformly distributed load, and thermal longitudinal expansion of the bridge deck were applied to the bridge models. Due to the nonlinear boundary condition used in the supports of the bridge model A, such as contact and friction, the superposition principle cannot be used in the calculations of this model. For this reason, all the loads involved in all bridge models were combined into a single load case and the large displacement formulation was used in the static analysis. The self-weight of the soil layer beneath the structure was omitted in the analysis. The author is focused on the method of modeling an integral bridge structure resting on elastic soil. For the purpose of this paper, only two piers from each model were selected, from which the internal forces and displacements were

compared. Based on the analysis, it was concluded that it is possible to design an integral bridge by building its simplified numerical model, once the conditions given in the conclusions are met.

Keywords: design; integral bridge; intermediate support; foundation stiffness; pier.

1 Introduction

An integral bridge can be defined as a bridge whose spans are monolithically connected with the intermediate supports and the abutment walls and whose structure interacts with the surrounding soil due to thermal effects and permanent and variable vehicle and pedestrian traffic loads. Elements such as bridge bearings, mechanical expansion joints, and approach slabs are not required in this case [1]. Therefore, the construction and maintenance of integral bridge are less expensive than for a conventional bridge containing the above-mentioned elements. Due to this, such a bridge becomes more environmentally friendly. Over the last few decades, the great popularity of integral bridge construction around the world has resulted in a significant number of highly valuable publications, of which only a few are mentioned in this paper [1] to [17]. One of them is the work of Polish researchers, professors K. Furtak and B. Wrana, entitled “Integral Bridges” [2]. The work focuses on general topics, such as the shaping, modeling and design of integral bridge structures. In publications [3] to [6], various aspects of the design and construction of integral bridges and viaducts (both single-span and multispan ones), arch bridges, and box bridges are described. The structures presented were designed by the author of this paper. In a report written by Lock [1], collated information on the earth pressures and settlements that develop behind model and full-scale integral bridge abutments is presented. The author of this work recommends gradually increasing the span length of newly designed integral bridges above the limit of 60 m that is recommended by British Standard [7]. Detailed information on the integral bridge maximum length

*Corresponding author: Andrzej Helowicz, Wrocław University of Science and Technology, Faculty of Civil Engineering, pl. Grunwaldzki 11, 50-370 Wrocław, Poland, E-mail: andrzej.helowicz@pwr.edu.pl, ORCID: <https://orcid.org/0000-0001-9527-1281>

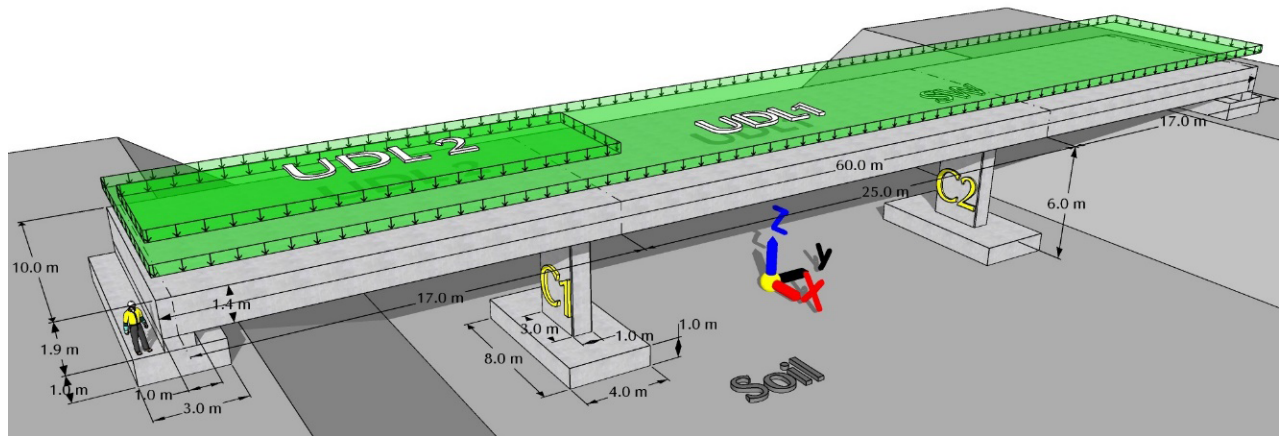


Figure 1: Analyzed integral bridge.

limits, as governed by flexural strength of abutments or by low-cycle fatigue performance of the piles, is provided by Pipinato et al. [8]. The authors of this handbook provide useful information about the most recent innovative construction practices and research in bridge engineering. For example, gravitational, thermal, and seismic effects in integral bridge structures are described. Furthermore, Nicholson [9] provided guidance and recommendations for the design of integral bridges, with an emphasis on the design of abutments. The guidance includes worked examples of integral bridge design using precast, prestressed bridge beams. In the article written by Biddle et al. [10], advice and guidance on the design of integral bridges that use steel in the composite deck, in the substructure, and also in both are presented. In the companion to this document, Way et al. [11] provide worked examples for a single-span fully integral bridge design. A design guide for composite bridges [12], written by European researchers in 2010, provides the main principles, technical solutions, and examples of technologies that are part of integral abutment systems. This document can be used by designers, engineers, building owners, and authorities during the whole design process. In addition, the document presents design examples including the basic design steps to assist the designer to carry out their own structure design. To improve the results of shallow foundation continuum models, the authors of the paper [13] investigated the contact stress distributions at the interface between the foundation and the underlying real homogeneous, dry, compacted sand. The research presented in [14], [15], and [16] focuses on the distribution of lateral stresses behind the abutment wall of the integral bridge structure, which are caused by seasonal expansion and contraction of the

bridge deck due to temperature fluctuations. The paper [17] presents a study of the seismic behavior and nominal capacity of a seven-span, 227 m long fully integral concrete railway bridge with an end-restraining abutment. The aim of this research was to determine the appropriate stiffness of the end-restraining abutment to withstand design earthquake loadings using a rigorous parametric study. A comprehensive literature review regarding the integral bridge structures and surrounding soil interaction is presented in [18]. The author of this work discusses various modeling methods for soil–structure interaction used in the design of the integral bridge structures that are primarily subjected to live loading and longitudinal thermal movements, and braking loads. Finally, in [19], Hambly provides simplified equations derived from elastic half-space theory to estimate the stiffnesses of the shallow footing foundations. The roots of these equations come from works written in the first half of the 20th century by the Russian scientists Gorbunov-Posadov [20], [21] and Barkan [22].

The above-mentioned publication [2], [18] and [19] shows many very difficult, not fully resolved topics related to the design of integrated bridges. One of the challenges encountered when designing an integral bridge structure is to accurately reflect the actual conditions of the bridge foundation in the numerical model. For this reason, the paper presents three methods of the numerical modeling of a 60 m long integral bridge resting on elastic soil (Fig. 1) and their impact on the values and distribution of displacements and internal forces in the bridge piers selected for analyses.

The abutment walls and the analyzed piers shown in Figure 1 are monolithically connected to the concrete bridge footing foundation and to the concrete bridge



The following section describes three numerical models of the analyzed bridge and the assumptions made in the models.

Complex model A consists of the bridge structure and the soil layer beneath it. In this model, the interlayer interaction between the bottom surface of the footing foundation and the top surface of the soil was modeled as a standard contact surface-to-surface type discretization method with a finite sliding formulation. Furthermore, normal behavior with “hard” contact pressure overclosure and allowable separation after contact was applied. The

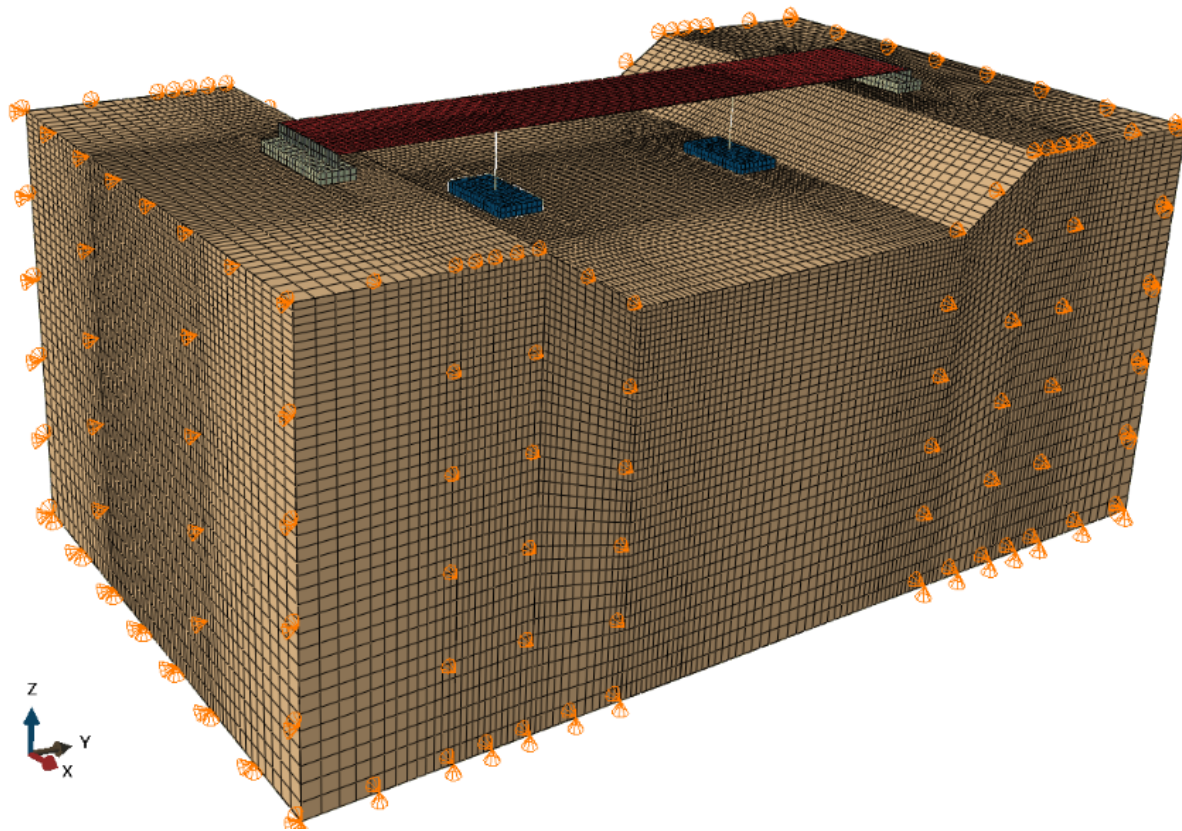


Figure 3: Finite element mesh of complex models A and C.



Figure 4: Finite element mesh of simple model B.

hard contact implies that the surfaces transmit no contact pressure unless the nodes of the slave surface contact the master surface and no penetration is allowed at each constraint location. The adopted contact method permits some relative motion of the contact surfaces. Contact interaction properties are a tangential behavior, with the static coefficient of friction μ being equal to 0.84. This coefficient was calculated based on the assumption that the internal angle of friction between concrete and soil material is the same as the internal angle of friction of the soil layer beneath the footing foundation. The simple model B consists of only the bridge structure. The missing layer of the soil in this model was replaced by spring constants derived for a rectangular foundation

resting on elastic half-space. Five spring constants were applied to the center of the bottom surface of each footing foundation. Three of them were responsible for vertical and horizontal motion, and the remaining two were responsible for rocking motion around the X- and Y- axis. Model B represents an engineering approach to the design of an integral bridge structure. The values of spring constants used in model B are shown in Table 1.

The third complex model C consists of the bridge structure and the soil layer beneath it. In this model, all sliding motion between the contact surfaces of the bridge foundation and the soil was prevented by applying an infinite coefficient of friction, which is named in Abaqus CAE software as “rough” friction surface interaction.

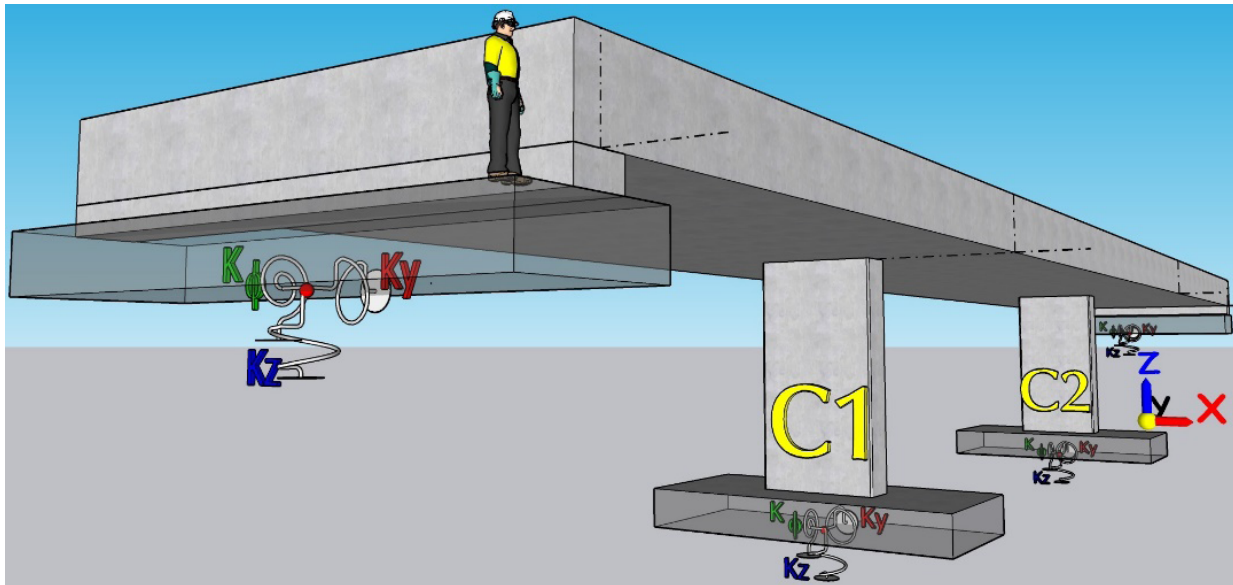


Figure 5: Location of the applied springs under the footing foundations in simple model B.

Table 1: Spring constants.

Element	Pier footing	Abutment footing
β_x (L/B)	L=8 m, B=4 m $\beta_x=0.944$	L=10 m, B=3 m $\beta_x=0.976$
β_y (L/B)	L=4 m, B=8 m $\beta_y=1.012$	L=3 m, B=10 m $\beta_y=1.096$
β_z (L/B)	L=4 m, B=8 m $\beta_z=2.175$	L=3 m, B=10 m $\beta_z=2.3$
$\beta_{\phi x}$ (L/B)	L=4 m, B=8 m $\beta_{\phi x}=0.435$	L=3 m, B=10 m $\beta_{\phi x}=0.402$
$\beta_{\phi y}$ (L/B)	L=8 m, B=4 m $\beta_{\phi y}=0.595$	L=10 m, B=3 m $\beta_{\phi y}=0.721$
k_x (kN/m)	427,021	427,819
k_y (kN/m)	457,832	480,236
k_z (kN/m)	560,860	574,345
$k_{\phi x}$ (kN/m/rad)	2,540,626	1,650,517
$k_{\phi y}$ (kN/m/rad)	6,944,437	9,854,189

In addition, the separation of contact surfaces in this model was blocked. Similar assumptions were made when deriving the equations for calculating the spring constants used in model B. The purpose of building the additional complex model C was to compare the computation results, such as the internal forces and displacements obtained from the complex model C, with the computation results obtained from model A, in which some relative motion of the contact surfaces between the footing foundation and the soil layer was permitted. In models A and C,

it was assumed that the soil layer beneath the structure has a constant, uniform depth of 32.0 m below the footing foundation of the piers and a depth of 37.5 m below the footing foundation of the abutment walls (Fig. 2). In all the numerical models, the bridge deck and the abutment walls are represented by 992 linear hexahedral shell elements of type S4. The S4 element is a four-node, double-curved general purpose shell element with preset element controls such as hourglass control parameter and finite membrane strains. Each pier consists of six Euler–Bernoulli two-node cubic beam elements of type B33. Kinematic type couplings were used to connect the beam elements with the solid elements (representing the footing foundation) and the shell elements (representing the bridge deck). In this connection, the bottom and top nodes of the beam elements were the control points, whereas the top surface of the footing foundation directly under the pier and the bottom surface of the deck directly over the pier were the constraint regions. These connections are shown in Figure 4. The footing foundation represents 992 general purpose eight-node linear hexahedral elements of type C3D8 with preset element controls such as hourglass control parameter. The same element type was used to build the block of the soil layer beneath the footing foundation. The total number of elements representing the soil layer beneath the footing foundation is equal to 392,616 elements. Material constants, such as the internal angle of friction (ϕ), Young’s modulus (E), and Poisson’s ratio (ν) of the materials selected for the analysis are presented in Table 2.

Table 2: Material properties used in the analysis .

Model	A, B, C
Soil	Loose sand and gravel [27]
E_s (MN/m ²)	80 (Middle range value)
ν	0.35
ϕ	40 (model A)
G (MN/m ²)	30.8
L (m)	3 and 4
B (m)	10 and 8
Bridge structure	Concrete C50/60
E_{cm} (MN/m ²)	37,000
ν	0.2

where: E – modulus of elasticity, ν – Poisson's ratio, ϕ – the soil's internal angle of friction, G – the soil's shear modulus, L – length of the foundation (in the plane of rotation for the case of rocking), and B – width of the foundation (along the axis of rotation for the case of rocking).

Table 3: Load applied to the structure.

Load type	Value
SW of the bridge structure SW	24 kN/m ³
UDL 1	10 kN/m ²
UDL 2	25 kN/m ²
The characteristic value of the maximum expansion range of the uniform bridge temperature component	$\Delta T_{N,exp} = 36^\circ\text{C}$

SW: self-weight, UDL: uniform distributed load

The soil's internal angle of friction was used only to calculate the coefficient of friction between the soil and the concrete surface, which was then used to simulate the contact interaction in model A. The dimensions of the footing foundation and the soil layer beneath the footing are shown in Figures 1 and 2. Each vertical surface of the soil layer has only a horizontal restraint applied perpendicularly to each surface. The bottom surface of this layer has only a vertical restraint applied perpendicularly to this surface. In addition, it was assumed that the footing foundation is not backfilled. This situation may occur during temporary works in the vicinity of the footing foundation. The nominal loads applied to the bridge structure are shown in Figure 1 and Table 3.

In model A, the superposition principle cannot be used in the calculations due to the nonlinear boundary

condition used in the supports of the bridge model, such as contact and friction. For this reason, all the involved loads in all bridge models were incorporated into a single load case, and the large displacement formulation was used in the static analysis. The characteristic value of the maximum contraction $\Delta T_{N,con}$ and the expansion range of the uniform concrete bridge deck temperature $\Delta T_{N,exp}$ were calculated according to Eurocode 1 [28]. In the analyses, it was assumed that the bridge would be built in Wrocław (Poland), where the annual maximum and minimum shade air temperature are equal to $T_{max} = 38^\circ\text{C}$ and $T_{min} = -32^\circ\text{C}$, and that the initial bridge temperature T_0 at which the structure will be cured shall be 5°C . For concrete bridge deck, the values of $T_{e,min} = -24^\circ$ and $T_{e,max} = 41^\circ$ were read from Figure 6.1 given in the Eurocode 1 [28]. The characteristic value of the maximum contraction and maximum expansion value of the uniform concrete bridge deck temperature were calculated from equations (6.1) and (6.2) found in the standard [28].

$$\Delta T_{N,con} = T_0 - T_{e,min} = [5^\circ - (-24^\circ)] = -29^\circ\text{C} \quad (2.1)$$

$$\Delta T_{N,exp} = T_{e,max} - T_0 = [41^\circ - 5^\circ] = 36^\circ\text{C} \quad (2.2)$$

The characteristic value of the maximum expansion value of the uniform concrete bridge deck temperature $\Delta T_{N,exp} = 36^\circ\text{C}$ was selected for the analysis. The earth pressure behind the walls of low-height abutments was omitted in the conducted comparative analysis.

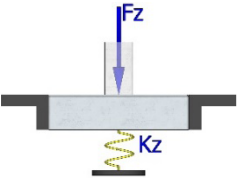
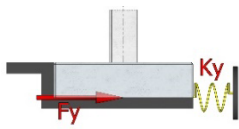
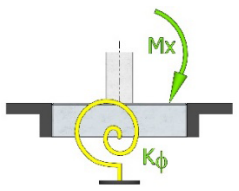
Section 3 describes the equations used to calculate the stiffness of springs used in model B. A detailed derivation of the described equations is given in [29].

3 Stiffness of shallow footing foundation

In model B, the stiffness of the soil layer beneath the bridge structure was replaced by the rocking, vertical, and horizontal springs applied to the bottom surface of the bridge shallow footing foundations. The stiffnesses of these springs were calculated from the equations given in [19], [22], and [26]. Equations (3.1) and (3.2), which are listed in Table 4, were derived by Russian scientist Barkan [22], whereas equation (3.3) was derived by Gorbunov-Possadov [20].

An extensive number of field tests, conducted by Barkan et al. [22], on the variety of soils and plate surfaces demonstrated the validity of the simplified method of modeling a foundation on elastic soil. The equations

Table 4: Equations for spring constants for a rectangular footing [21], [22].

Spring constants	Motion	Reference
Vertical stiffness $k_z = \frac{G}{(1-\nu)} \beta_z \sqrt{BL} \quad (3.1)$		Barkan (1962)
Horizontal stiffness $k_y = 2(1+\nu)G\beta_y \sqrt{BL} \quad (3.2)$		Barkan (1962)
Rocking stiffness $k_\phi = \frac{G}{(1-\nu)} \beta_\phi BL^2 \quad (3.3)$		Gorbunov-Posadov (1961)

where: L – length of foundation (in the plane of rotation for the case of rocking), B – width of foundation (along the axis of rotation for the case of rocking), ν – the soil's Poisson's ratio, G – the soil's shear modulus, $(\beta_y, \beta_z, \beta_\phi)$ – spring coefficients, and (k_y, k_z, k_ϕ) – spring constants.

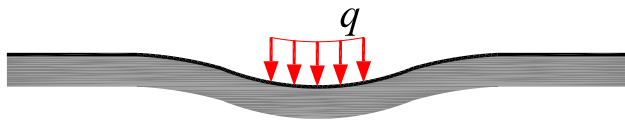


Figure 6: Actual soil deformation and according to the theory of elasticity.

provided by Posadov-Gorbunov [20], [21] and Barkan [22] were derived for a rectangular shallow footing foundation from the theory for an elastic half-space. According to this theory, the ground is treated as a continuous, homogeneous, and elastic body extending infinitely far down and to the sides and is limited from above by a plane (Fig. 6).

The equations in Table 4 have been used since the 1960s in the design of concrete foundations for heavy industrial machinery that induces additional dynamic loads [22], as well as in the design of integral bridge structures [19]. The equations for calculating the spring stiffness were derived based on the following main assumptions [21] and [22]:

1. The footing foundation is embedded in a shallow excavation. Therefore, the effect of the depth of excavation on which the footing foundation is resting is not taken into account.
2. The effects described in [30] and [31], such as the plasticization and the rheological behavior of the

subsoil, and the need to include them in the design process were not taken into account.

3. The footing foundation is assumed to adhere tightly to the soil – even under negative pressure.
4. All forces and bending moments act in the center of the footing foundation.
5. The values of the soil coefficients are determined according to the allowable pressure of the footing foundation on the soil and not according to the actual pressure. However, in reality, there is no such dependency.
6. It is assumed that the pressure on the soil is much lower than the load-bearing capacity of the soil.
7. The effect of ground inertia is not included in the calculations.

The self-weight of the soil beneath the structure (“effective mass”) was omitted in the analysis. Exclusion of the mass of the soil in the analyzed models was explained by Whitman and Richard in 1967 [25]. According to their work, the mass of an equivalent lumped system should at least include the mass of the machinery and mass of the foundation block. It seems that the mass of the soil under the foundation involved in the movement should also be included in the equivalent lumped system. However, there is no well-defined mass of soil that moves with the same amplitude and in phase with the foundation block.

At a given moment, different parts of the soil are moving in different directions and with different magnitudes of acceleration. Taking this effective mass into account is only justified by the fact that the interaction curve of the equivalent system is consistent with the interaction curve of the real system. It is known that the effective mass is greater than the mass of the foundation block and the machine. If effective mass is used in calculations, it should be noted that it represents a completely fictitious number that cannot be related to the actual mass of the soil. The simplest assumption that can be made when selecting the mass of the equivalent system is to consider only the machine and the foundation and to ignore any effective mass of the soil. In addition, the use of the modulus of elasticity of soil in this method was explained by Gorbunov-Posadov [21]. When the soil is subjected to repeated loading, the inelastic deformations disappear over time and the modulus of the deformation of soil changes into the modulus of elasticity E_s , the value of which is usually much higher.

The spring constant coefficients β_y , β_z , and β_ϕ used in equations 3.1, 3.2, and 3.3 depend on the ratio of the L/B of the footing foundation's dimensions. In addition, coefficient β_y depends on the value of Poisson's ratio ν . Gorbunov-Posadov [21] and Barkan et al. [22] do not provide both the equations for determining the spring coefficients and the derivations of the equations for determining the spring constants. Thus, based on the assumptions provided by Barkan and Gorbunov-Posadov, the equations for the spring constants k_y , k_z , and k_ϕ and the spring coefficients β_y , β_z , and β_ϕ were derived and their final form is presented in this paper.

$$\beta_y = - \frac{3\pi\alpha^{\frac{3}{2}}}{2(\nu+1) \left[3\alpha^2(\nu-1)\ln\left(\frac{\sqrt{\alpha^2+1}+1}{\alpha}\right) - 3\alpha\ln(\sqrt{\alpha^2+1}+\alpha) \right] - \frac{3\pi\alpha^{\frac{3}{2}}}{-v(\sqrt{\alpha^2+1} \cdot (2\alpha^2-1) - 2\alpha^3+1) + (\alpha^2+1)^{\frac{3}{2}} - \alpha^3 - 1}} \quad (3.4)$$

$$\beta_z = \frac{\pi\alpha^{\frac{3}{2}}}{\frac{1}{2}\alpha^2\ln\left(\frac{(\sqrt{\alpha^2+1}+1)^2}{\alpha^2}\right) + \alpha\ln(\sqrt{\alpha^2+1}+\alpha) - \frac{1}{3}((\alpha^2+1)^{\frac{3}{2}} - \alpha^3 - 1)} \quad (3.5)$$

$$\beta_\phi = A_{10}\alpha^{10} + A_9\alpha^9 + A_8\alpha^8 + A_7\alpha^7 + A_6\alpha^6 + A_5\alpha^5 + A_4\alpha^4 + A_3\alpha^3 + A_2\alpha^2 \quad (3.6)$$

$$+ A_1\alpha + A_0$$

where:

$$\begin{aligned} A_0 &= 0.315, & A_1 &= 0.411, & A_2 &= -0.5154, \\ A_3 &= 0.4464, & A_4 &= -0.2236, & A_5 &= 6.88855E-02, \\ A_6 &= -1.34905E-02, & A_7 &= 1.6845E-03, & A_8 &= -1.29857E-04, \\ A_9 &= 5.63104E-06, & A_{10} &= -1.05042E-07 \end{aligned}$$

The parameter $\alpha=L/B$ in equations (3.4)–(3.6) is the ratio of L the length of the foundation (in the plane of rotation for the case of rocking) to B the width of the foundation (along the axis of rotation for the case of rocking). For all spring coefficients, the value of the parameter $\alpha=L/B$ varies from 0.1 to 10.

Equations (3.4) and (3.5) were derived based on the equations given by Barkan [22]. In addition, equation (3.6) was derived in the form of a polynomial of the 10th degree because the values of the parameters K_1 and K_2 given by Gorbunov-Posadov [20] for calculating the spring coefficient β_ϕ , should be read from the graphs. In Section 4, a comparative analysis of the numerical models of the integral bridge is presented.

4 Comparative analysis

The subjects of the analysis were piers C1 and C2, presented in Figure 1. In each of these piers, the values and distribution of the internal forces and displacements obtained from bridge models A, B, and C were compared and analyzed.

4.1 Bending moments

The graphs showing the values and distribution of bending moments M_x and M_y in piers C1 and C2 in all the analyzed bridge models are shown in Figure 7.

The following conclusions can be drawn from the comparative analysis of the bending moments in piers C1 and C2 in bridge models A, B, and C:

1. The values of bending moment M_x in pier C1 in simple model B are higher than in complex models A and C. The values of bending moment M_x in pier C2 in models B and C are similar.
2. The values of bending moment M_y in simple model B differ from the values of the bending moments in complex models A and C by a maximum of 8.4%.

4.2 Shear forces

The graphs showing the values and distribution of shear and axial forces T_x , T_y , N_z in piers C1 and C2 in all the analyzed bridge models are shown in Figure 8.

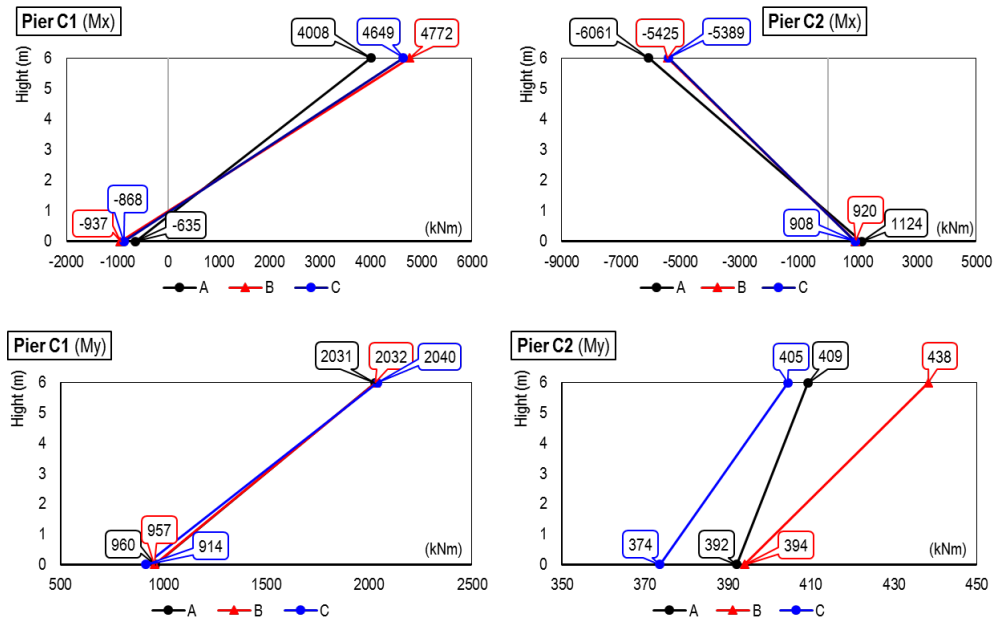


Figure 7: Bending moments in piers C1 and C2 where *A* and *C* are complex bridge models and *B* is a simple bridge model.

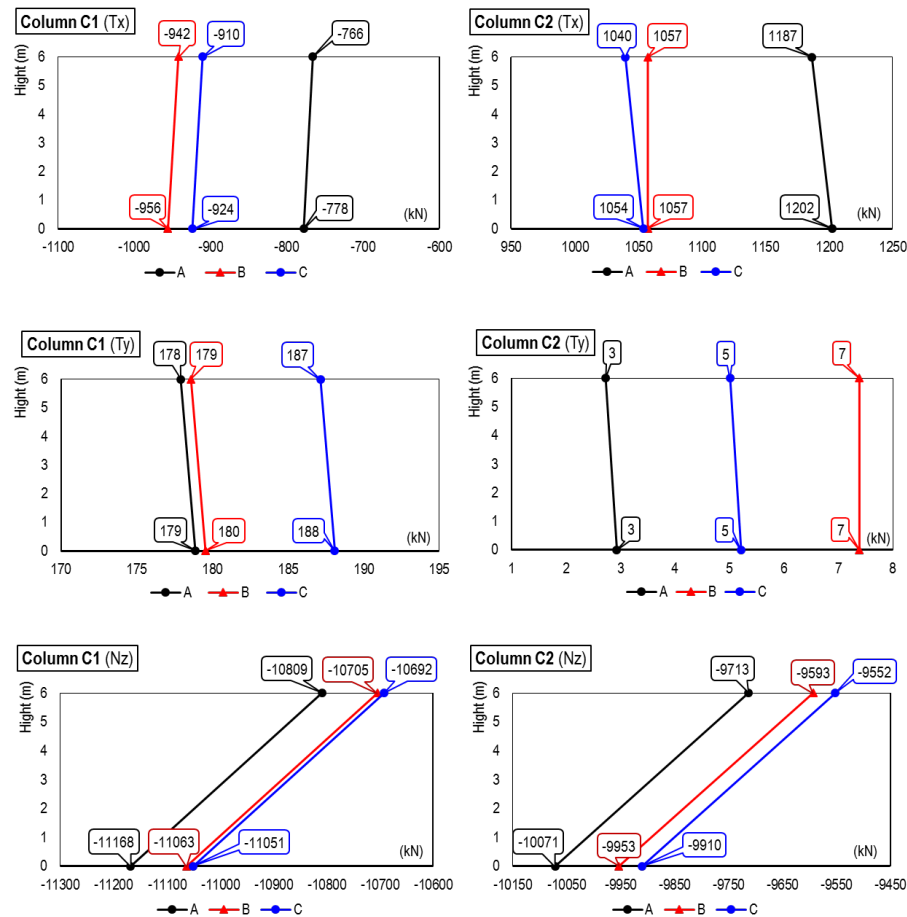


Figure 8: Shear and axial forces in piers C1 and C2.

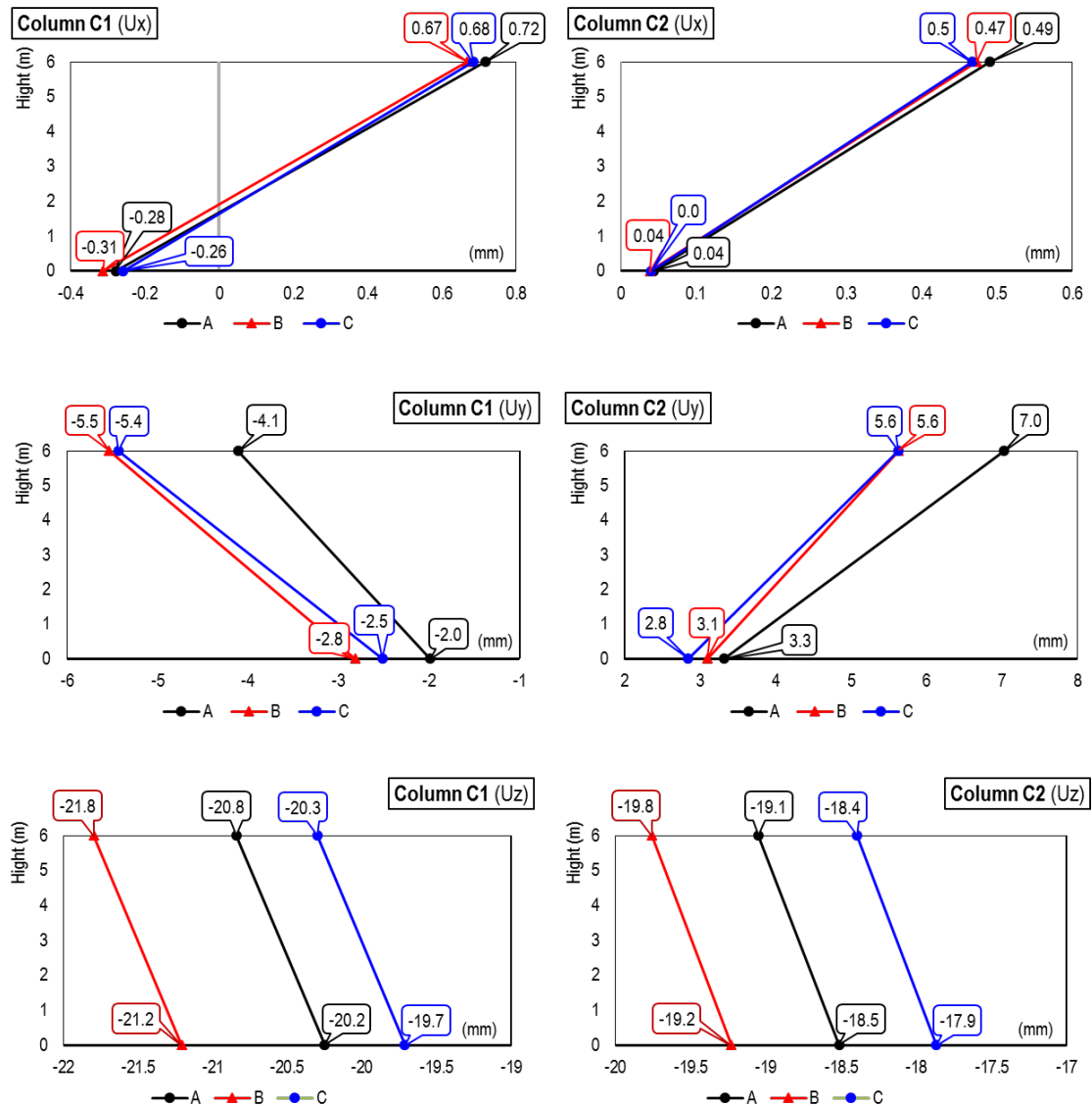


Figure 9: Horizontal and vertical displacements in piers C1 and C2 where U_x and U_y are horizontal displacements along the X-axis and Y-axis direction and U_z is the vertical displacement along the Z-axis direction.

The following conclusions can be drawn from the comparative analysis of the shear and axial forces in piers C1 and C2 in bridge models A, B, and C:

1. The axial force N_z in the piers in simple model B differs by approximately 1% from the axial force in both piers in complex models A and C.
2. The shear force T_x in pier C1 in simple model B is higher by approximately 23% than in complex model A and is about 3.5% higher than in complex model C. The opposite is true in pier C2.
3. The shear force T_y in pier C1 in simple model B is lower by approximately 12% than in complex models A and C. In addition, the shear force T_y in pier C2 in simple model B is higher than in complex models A

and C. Finally, the shear forces T_y in pier C2 in simple model B differ by a maximum of 4 kN from the values of these forces in pier C2 in complex models A and C.

4.3 Horizontal and vertical displacement

The graphs showing the values and distribution of the displacements of piers C1 and C2 in all the analyzed bridge models are shown in Figure 9.

The comparative analysis of displacements of piers C1 and C2 in bridge models A, B, and C shows the following:

1. The displacements of piers C1 and C2 in all the bridge models are very similar.

2. The vertical displacement U_z in piers C1 and C2 in simple model B is higher by a maximum of 1.5 mm than the displacement in the piers of complex models A and C.
3. The horizontal displacement in the Y-axis direction of pier C1 in simple model B is greater than the displacement of pier C1 in complex models A and C.

5 Conclusions

The method used to calculate the displacement and internal forces in simple model B (in which the stiffness of the soil layer beneath the bridge structure was replaced by the rocking, vertical, and horizontal springs applied to the bottom surface of the bridge footing foundations) could be used for preliminary bridge design. To use this method in the design of the integral bridge structure, it is necessary to rectify the spring coefficients β_y , β_z , and β_ϕ used to calculate the spring constants k_y , k_z , and k_ϕ given in equations 3.1, 3.2, and 3.3. In simple model B, it was assumed that the overall depth of the soil under the foundation has uniform stiffness, while in reality, such a situation occurs very rarely. In nature, a typical soil consists of layers of different thicknesses and stiffnesses. For this reason, it is necessary to build a complex bridge model (similar to model A) that takes into account the bridge structure, the stiffness of the individual layers of the soil on which the bridge is resting, and the interaction of the footing foundation and soil layer under the footing. A complex bridge model can be used in preliminary bridge design to calibrate the spring constants k_y , k_z , k_ϕ that can be applied in a simple bridge model. This can speed up the design process and reduce the amount of redundant data. It is worth noting that despite the significant difference in building the simple model B consisting of 3444 elements, and the complex models A and C consisting of 396,060 elements each and in which, the contact between the foundation surface and the soil layer beneath it was additionally modeled, the calculated values of bending moments, shear forces, and displacements are similar in all analyzed models. This is especially noticeable when comparing the simplified model B and model C, in which all sliding motion between the contact surfaces of the bridge foundation and soil is prevented. Therefore, in some cases, the method used in simple model B could be used in the design of small and medium-sized integral bridge structures. An additional argument in favor of using a simplified model for bridge structure design, as in the example of bridge model B, is the fact that the time

required to conduct the calculations of simple model B was 1 minute, whereas the time required to conduct the calculations of complex model A was 210 min. In addition, the output database file from model A contains 4.38 GB of data, with model B containing only 7.1 MB of data. The complex models A and C can be further optimized, potentially speeding up their calculation time. However, the paper presents a simple bridge model with one set of loads, whereas in practice, more complex bridge models can be found, and the proposed simplified modeling method used in bridge model B will be far more beneficial due to its simplicity and much shorter calculation time. It should be emphasized that before design calculations that take stiffness of soil layer beneath the structure into account, the proper soil parameters for both soil and backfill must be determined. On the basis of such data, a designer can build a numerical model of a structure resting on soil with a specific stiffness. Therefore, close cooperation is required between a geotechnical engineer and structural engineer when designing integral bridges. Finally, it should be noted that the implementation of integral bridges and viaducts on motorways in Ireland, in which the author was involved in the design as a senior structure design engineer, contributed to a significant reduction in the time and cost of their construction.

Acknowledgements

The calculations were carried out using resources provided by Wrocław Center for Networking and Supercomputing (<https://wcoss.pl>), grant No. 554.

References

- [1] Lock R. J. (2002). Integral Bridge Abutments. CUED/D-SOILS/TR320.
- [2] Furtak K., Wrana B. (2005). Mosty zintegrowane. Wydawnictwo komunikacji i łączności Warszawa, ISBN: 832061550X.
- [3] Helowicz A. (2017). Wieloprzęsłowe wiadukty zintegrowane z przęslami skrzynkowymi – doświadczenie projektanta. *Acta Scientiarum Polonorum. Architectura*, vol. 16, no. 3, (pp. 107-117).
- [4] Helowicz A. (2020). Integral bridge and culvert design, Designer's experience. *Open Engineering*, (Vol. 10, no. 1, Jun 2020).
- [5] Helowicz A. (2021). Impact of subgrade and backfill stiffness on values and distribution of bending moments in integral box bridge, *Studia Geotechnica et Mechanica*, (Vol. 43, nr 2, pp. 90-98).

- [6] Helowicz A. (2024). Modelling of foundation stiffness beneath intermediate support of 178 m long integral viaduct. *Archives of Civil Engineering*. No. 2/2024.
- [7] BA42/96 (2003), The Design of Integral Bridges. Design Manual for Roads and Bridges, Volume 1, Section 3, Part 12. The Stationery Office, London, UK.
- [8] Pipinato A. et al. (2022). Innovative Bridge Design Handbook, Construction Rehabilitation and Maintenance, Second Edition. *Butterworth-Heinemann is an imprint of Elsevier*, ISBN 9780128235508.
- [9] Nicholson B. A. (1998). Integral abutments for prestressed beam bridges. *Prestressed Concrete Association*, ISBN 0950034770.
- [10] Biddle A. R., Iles D. C., Yandzio E., (1997). Integral Steel Bridges – Design Guidance. *The Steel Construction Institute Publication*, SCI P163, ISBN 1859420532.
- [11] Way J. A., Yandzio E. (1997). Integral Steel Bridges. Design of a Single-Span Bridge – Worked Example. *The Steel Construction Institute Publication*, SCI P180. ISBN 1859420567.
- [12] Feldmann M., Naumes J., Pak D. et.al (2010). Economic and Durable Design of Composite Bridges with Integral Abutments – Design Guide. *RFCS publications*. ISBN 978-92-79-22157-6.
- [13] Taylor, A.G.; Chung, J.H. (2022). Explanation and Application of the Evolving Contact Traction Fields in Shallow Foundation Systems. *Geotechnics*, (Vol. 2), 91-113. Available: <https://doi.org/10.3390/geotechnics2010004>.
- [14] Luo S. De Luca F. De Risi R. et al. (2022). Challenges and perspectives for integral bridges in the UK: PLEXUS small-scale experiments. *ICE Publishing*. Available: <https://doi.org/10.1680/jsmic.21.00020>
- [15] Stastny A., Stein R., Tschuchnigg F. (2022). Long-term monitoring of the transition zone of an integral railway bridge in Germany. International Symposium 11th Field Monitoring in Geomechanics.
- [16] Stastny A., Knittel L., Meier T. Tschuchnigg F. (2022). Experimental determination of hypoplastic parameters and cyclic numerical analysis for railway bridge backfills. *Acta Geotechnica*, Springer.
- [17] Reddy B. R., Reddy Ch. S. (2020). Seismic Performance Evaluation of a Fully Integral Concrete Bridge with End-Restraining Abutments. *Journal of Engineering Sciences*. (Vol.11, Issue2), ISSN NO: 0377-9254.
- [18] Featherston. N., R. (2022). Parametric modelling of integral bridge soil spring reactions. Thesis for the degree of Master of Engineering (Research) in the Faculty of Civil Engineering at Stellenbosch University.
- [19] Hambly E. C. (1991). Bridge deck behaviour, 2nd ed. *E & FN Spon*, London and New York.
- [20] Gorbunov-Posadov M. I. (1949). Балки и плиты на упругом основании. Издательство Министерства Строительства Предприятий Машиностроения, Москва.
- [21] Gorbunov-Posadov M. I. (1956). Obliczenie konstrukcji na podłożu sprężystym. *Wydawnictwo Budownictwo i Architektura*. Warszawa.
- [22] Barkan D. D. (1962). Dynamics of Bases and Foundation. *The McGraw-Hill Book Company*, New York, USA.
- [23] PN-EN 1992-1-1. (2008). Projektowanie konstrukcji z betonu. Część 1-1: Reguły ogólne I reguły dla betonów. PKN.
- [24] Abaqus FEA Software, “Abaqus analysis user’s manual”, Version 2016, Dassault Systemes. [Online]. Available: <http://130.149.89.49:2080/v2016/index.html>.
- [25] Lambe T.W., Whitman R.V. (1969). Soil Mechanics. *John Wiley*, New York, USA.
- [26] Richart F. E., Hall J. R., Woods R. D. (1970). Vibrations of Soils and Foundations. *Prentice-Hall*, New Jersey, USA.
- [27] Bowles J. E. (1997). Foundation analysis and design. Fifth Edition. *The McGraw-Hill Companies, Inc.* ISBN 0079122477, New York USA.
- [28] PN-EN 1991-1-5. (2005). Oddziaływania na konstrukcje. Część 1-5: Oddziaływania ogólne. Oddziaływania termiczne. PKN.
- [29] Pakos W., Helowicz A. (2024). Theoretical and numerical modeling of a shallow foundation stiffness based on the theory of elastic half-space. The publication is accepted for publication in the journal *Studia Geotechnica et Mechanica*.
- [30] Kuczma S. M., Świtka R. (1990). Bending of elastic beams on Winkler-type viscoelastic foundations with unilateral constraints. *Computers and Structures*, vol. 34, no 1, 125–136.
- [31] Kuczma S. M. (1999). A viscoelastic-plastic model for skeletal structural systems with clearances. *Computer Assisted Mechanics and Engineering Sciences*, no 6, 83–106.